Dielectric Absorption Caused by Traps in MIM/MOS Capacitors: A New Model Validated Through TCAD

Simone Saro, Pierpaolo Palestri, *Senior Member, IEEE*, Enrico Caruso, Paolo Toniutti, and Francesco Driussi, *Member, IEEE*

***Abstract*— We propose here a flexible physics-based model to calculate the capacitance and conductance in MIM and MOS capacitors, accounting for traps with different energy and space distributions in the dielectric. The proposed model is validated against calibrated TCAD simulations. Furthermore, the frequency and temperature dependencies of the loss tangent obtained from the TCAD simulations have been analyzed and compared with experimental trends reported in the literature, highlighting their relation with the trap location in the oxide and the electron trapping process. These findings offer insight into the trap-induced effects in MIM capacitors, helping to determine the physical origin of the dielectric absorption (DA) phenomenon affecting relevant CMOS circuits such as analog-to-digital converters (ADCs).**

***Index Terms*— Capacitance, conductance, dielectric absorption (DA), oxide traps, tangent of the loss angle.**

I. Introduction

MIM and MOS capacitors are extensively used as fundamental building blocks in analog, RF, and mixed signal ICs for a wide range of applications. Among these, this work focuses on analog-to-digital converters (ADCs), where MIM capacitors are employed to sample the analog data. Due to this, the ADCs performance is affected by the dielectric absorption (DA) effect [1], [2], [3], [4], a physical mechanism occurring in the capacitors which results in the frequency dispersion of the capacitance value and limiting the resolution and the achievable number of bits of the ADC. Even if different physical mechanisms (such as dipoles or Maxwell–Wagner interfacial polarization) may impact the frequency dependence of the permittivity [5], [6], [7], in CMOS technologies the DA is often associated with the presence of border traps in the dielectric [8], [9], [10], [11], [12]. In particular, DA induces a decreasing capacitance C and an increasing parallel conductance G with increased applied AC signal frequency [9], [13], [14], which results into the specific frequency trends of the measured tangent of the loss angle ($\tan\delta = G/\omega C$) observed in the literature [15], [16], [17], [18], [19], [20], [21], [22], [23], [24] and reported in Fig. 1. Although other figures of merit can be used to monitor the DA (e.g. the Voltage coefficients of the capacitance), this work focuses on $\tan\delta$, since it is strictly related to the capacitor quality factor ($Q = 1/\tan\delta$) and it is the key parameter for describing the DA effects on ADC operation as demonstrated in [2].

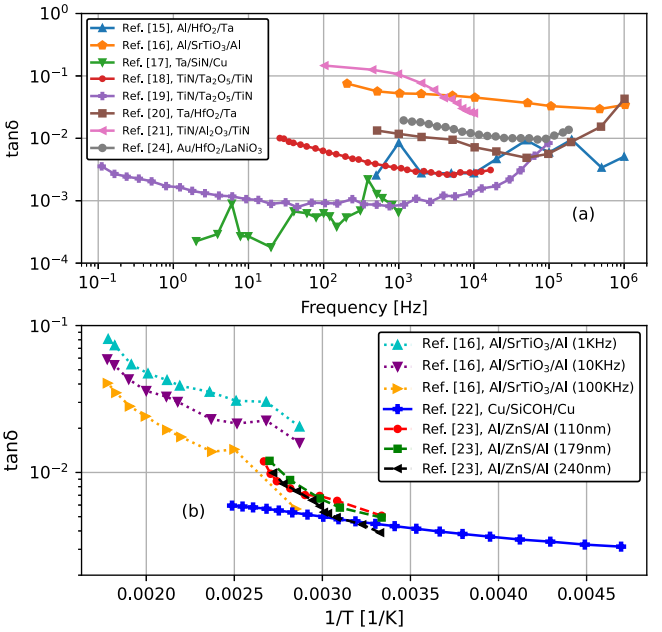

Fig. 1. (a) Experimental tangent of the loss angle reported in the literature versus the measurement frequency. Note that the $\tan\delta$ increase at high frequency shall be attributed to the effect of unwanted series resistances [23], [25], [26]. (b) Arrhenius plot of the experimental $\tan\delta$ from the literature, showing an increasing $\tan\delta$ with the temperature T. The large variance of values and trends over frequency and T may originate from different trap distributions in energy and space, as well as from the different dielectric materials (reported in the legend).

Received 19 May 2025; revised 16 October 2025 and 10 November 2025; accepted 11 November 2025. Date of publication 27 November 2025; date of current version 6 January 2026. The review of this article was arranged by Editor S. Harada. *(Corresponding author: Simone Saro.)*

Simone Saro and Francesco Driussi are with DPIA, University of Udine, 33100 Udine, Italy (e-mail: saro.simone001@spes.uniud.it).

Pierpaolo Palestri is with the Engineering Department "Enzo Ferrari," University of Modena and Reggio Emilia, 41125 Modena, Italy.

Enrico Caruso and Paolo Toniutti are with Infineon Technologies Austria, 9500 Villach, Austria.

Digital Object Identifier 10.1109/TED.2025.3633623

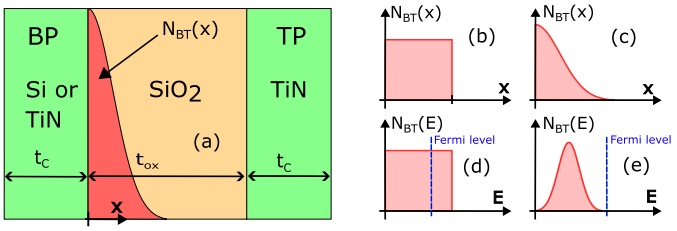

Fig. 2. (a) Simulated structure consisting of a TP of TiN, a BP of either TiN or Si with t_c = 20 nm and a SiO_2 region of t_{ox} = 30 nm. The trap distribution $N_{BT}(x, E)$ could be uniform (b) or Gaussian (c) in space and uniform (d) or Gaussian (e) in energy.

In Fig. 1, the spread of the $\tan\delta$ values and of the corresponding trends over frequency [Fig. 1(a)] and temperature (b) suggests that the DA in different capacitors/dielectrics originates from traps having different concentrations, as well as different distributions in space and energy [27].

Hence, $\tan\delta$ and its dependency on the device architecture, material, and measurement conditions may be considered as a monitor of the trap-related effects causing the DA. Therefore, it is useful to investigate how various trap distributions impact $\tan\delta$ and, thus, the circuits/systems deploying the capacitors.

In the past, DA has been routinely modeled through the equivalent resistance-capacitance model proposed by Dow et al. [28], which, however, does not provide physical insight into the DA origin. Instead, Yuan et al. [29] proposed a circuit model to describe the DA in a MOS capacitor affected by traps distributed along the dielectric and exchanging carriers only with the semiconductor substrate. The model is based on the following differential equation, whose solution [obtained by integration along the direction x, Fig. 2(a)] describes the total admittance of the MOS device:

$$\frac{dY}{\mathrm{dx}} = -\frac{Y^2}{j\omega\varepsilon_{\mathrm{ox}}} + \frac{j\omega q^2 N_{\mathrm{BT}}(x)}{1 + j\omega\tau(x)} \tag{1}$$

where ε_{ox} is the oxide permittivity, N_{BT} is the trap density per unit area and energy, and τ is the time constant associated with the charge exchange between traps and the semiconductor. In a MOS device, this equation must be numerically solved with the boundary condition $Y(x = 0) = j\omega C_S$, where C_S is the semiconductor capacitance. Equation (1) accounts only for the traps whose energy is aligned with the Fermi level in the bulk semiconductor, and it does not consider the band bending associated with the electric field in the oxide due to the bias applied to the capacitor when calculating the trap response to the AC signal. The assumption that charge can only be exchanged between traps and the semiconductor prevents the application of this model to MIM capacitors, where traps typically exchange charge with both electrodes.

To overcome the limits of the model of [29], we here propose a new model based on explicit integrals to calculate the capacitor admittance when traps communicate with *both electrodes* and are *non-uniformly distributed in space and energy*, thus allowing to reproduce various $\tan\delta$ trends over frequency and temperature. Furthermore, we avoid the use of empirical fitting parameters by employing state-of-the-art expressions for the elastic and phonon-assisted electron tunneling between electrodes and traps. The model is validated through extensive comparison with TCAD simulations of MIM and MOS capacitors with defective dielectrics.

The manuscript proceeds as follows. Section II describes the analyzed devices, the trap distributions and the TCAD simulation framework; Section III derives the model proposed to calculate the capacitance and conductance in the presence of traps; Section IV compares the model with the TCAD simulations for different trap distributions in energy and space and with experiments.

II. Analyzed Devices and TCAD Simulation Models

Fig. 2(a) sketches the studied device, highlighting the different trap distributions $N_{BT}(x, E)$ considered in our analysis. The capacitors have a 20-nm TiN top plate (TP), a 30-nm SiO_2 region, and a 20-nm bottom plate (BP). This latter can be composed either by TiN or Si, thus obtaining a MIM or a MOS capacitor, respectively. Concerning $N_{BT}(x, E)$, Fig. 2(b) and (c) report template spatial trap distribution interacting only with the BP in the TCAD simulations: 1) a uniform one extending 5 nm from the BP/SiO_2 interface and 2) a Gaussian profile centered at the BP/SiO_2 interface with σ = 1 nm. Similar distributions can also be placed close to the other electrode, thus having traps that exchange charge with the TP. In energy, we considered traps either uniformly distributed over 2 eV [Fig. 2(d)] or distributed as a Gaussian profile with σ = 1 eV [Fig. 2(e)]. In both cases, the energy distribution is centered 0.5 eV below the BP Fermi level.

For TCAD simulations, we used the Synopsys Sentaurus tool [30] (version W-2024.09). For trapping, we considered either elastic or inelastic tunneling processes. For elastic tunneling, the capture rate between one of the two electrodes and a trap at position x is calculated as [30]

$$c = \frac{\sqrt{8m_t}m_0^{3/2}g_C V_T}{\hbar^4\pi}(E_C(x) - E)^2\,\theta[E - E_C(0)]\cdot \\ \cdot\sqrt{E - E_C(0)}\,f\left(\frac{E_F - E}{kT}\right)\frac{|\Psi(x,E)|^2}{|\Psi(0,E)|^2} \tag{2}$$

where m_t and m_0 are the tunneling and free electron masses, respectively, g_C is the prefactor of the Richardson constant, V_T and E are the trap volume and energy, E_F is the Fermi level in the electrode, $E_C(x)$ is the SiO_2 conduction band (CB) bottom at the trap position x, while $E_C(0)$ is the semiconductor CB minimum at the interface (if the electrode is TiN this values defaults to −11.7 eV), θ is the step function, T is the temperature, and k is the Boltzmann's constant.

For inelastic tunneling we use [30], [31]

$$c = \frac{\sqrt{m_t m_0^3 k^3 T^3}g_C V_T S\hbar\omega}{\hbar^4\sqrt{\chi}}\exp\left[-S(f_B + 1) + \frac{\Delta E}{2kT} + \chi\right]\cdot \\ \cdot\left(\frac{z}{l+z}\right)^l F_{1/2}\left(\frac{E_F - E_C(0)}{kT}\right)\frac{|\Psi(x,E)|^2}{|\Psi(0,E)|^2} \tag{3}$$

where S is the Huang–Rhys factor, $\hbar\omega$ is the phonon energy, $f_B = [\exp(\hbar\omega/kT) - 1]^{-1}$ is the Bose–Einstein occupation, $z = 2S(f_B(f_B + 1))^{1/2}$, l is the number of phonons involved in

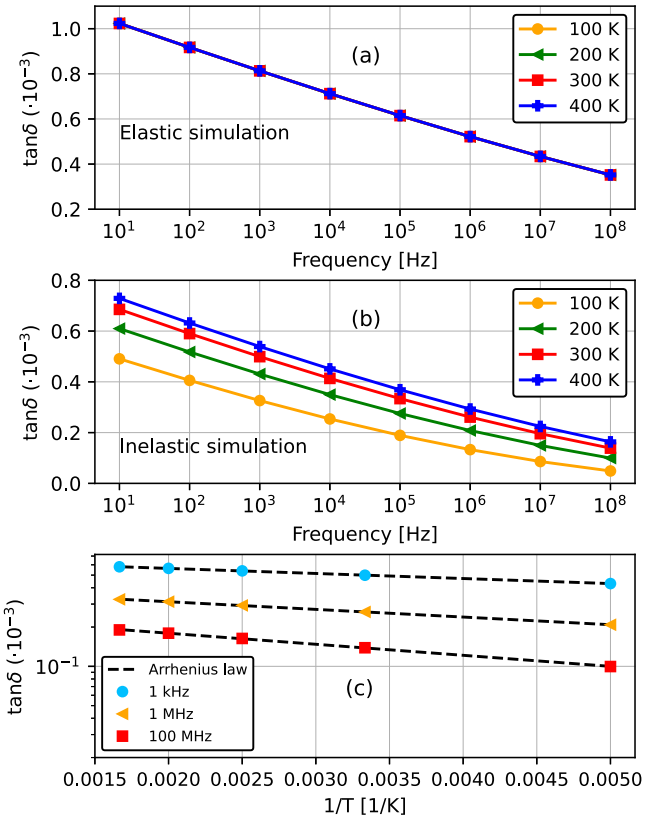

Fig. 3. TCAD simulations of $\tan\delta$ of the MIM stack in Fig. 2(a) with uniform $N_{BT} = 10^{19}$ eV^{-1}cm^{-3} by using (a) elastic or (b) inelastic tunneling. Only for inelastic tunneling, $\tan\delta$ increases with T as in Fig. 1(b). (c) Arrhenius plot of the data in (b) fit with the Arrhenius law (dashed lines) by using the parameters: $A_{1\text{ kHz}} = 0.672$, $E_{A\,1\text{ kHz}} = 7.69$ meV, $A_{1\text{ MHz}} = 0.409$, $E_{A\,1\text{ MHz}} = 11.7$ meV, $A_{100\text{ MHz}} = 0.265$, and $E_{A\,100\text{ MHz}} = 16.8$ meV. Traps exchange electrons only with the BP and are uniform in energy and space [Fig. 2(b) and (d)].

trapping, $\chi = (l^2 + z^2)^{1/2}$, $\Delta E = E_F - E$. In (2) and (3)

$$\frac{|\Psi(x,E)|^2}{|\Psi(0,E)|^2} = \frac{v(0,E)}{v(x,E)}\Gamma_{cc}(x,E) \tag{4}$$

where Γ_{cc} is the tunneling probability calculated with the WKB approximation and $v(x,E)$ is the electron velocity inside the trap calculated as

$$v(x,E) = \sqrt{\frac{2[E - E_C(x)]}{m_t m_0}} \tag{5}$$

and $v(0,E)$ is the electron velocity in the BP/TP. For the MOS stack, $v(0,E)$ is computed by using (5) at the energy $E_C(0)$. For the MIM stack, instead, $v(0,E) = v(x,E)$. Note that the capture rate c is related to the time constant τ in (1) through the Fermi function f_0 in the electrode as [32]

$$\tau(x,E) = \frac{f_0(E)}{c(x,E)}. \tag{6}$$

Table I lists the parameters used in the TCAD simulations, while Fig. 3(a) presents the typical $\tan\delta$ simulated with TCAD for a MIM with traps uniformly distributed in space and energy as in Fig. 2(b) and (d) ($N_{BT} = 10^{19}$ eV^{-1}cm^{-3}) and by considering elastic tunneling. Although the frequency dependence is qualitatively consistent with the experiments in Fig. 1(a), the simulated $\tan\delta$ does not depend on temperature in contrast with the measurements in Fig. 1(b).

TABLE I
PARAMETERS OF THE SiO_2 DIELECTRIC USED IN THE TCAD SIMULATIONS OF THE DEVICES REPORTED IN FIG. 2

m_t	$\hbar\omega$	S	V_T	g_C	$Voltage$
-	$[meV]$	-	$[cm^3]$	-	$[V]$
0.42 [33]	46 [34]	13 [35]	10^{-23} [35]	2.1 [30]	0

Conversely, Fig. 3(b) shows the TCAD simulation for the same MIM structure and trap distribution, but considering inelastic tunneling. Now, $\tan\delta$ exhibits a clear increase with temperature, similar to the experiments in Fig. 1(b), while maintaining the decreasing trend over frequency. Hence, the inelastic process results in being the only tunneling mechanism consistent with the experimental finding, and thus, all the following simulations are carried out considering only inelastic tunneling. Fig. 3(c) shows the Arrhenius plot of the $\tan\delta$ in Fig. 3(b) at three different frequencies (symbols). TCAD curves show a good agreement with the Arrhenius law $A \cdot e^{-E_A/kT}$ (dashed lines), qualitatively consistent with the data in Fig. 1(b).

To show that the TCAD results agree with DA models such as the one in [29], we compare (1) with simulations considering a uniform $N_{BT} = 10^{17}$ eV^{-1}cm^{-3} in energy and space [Fig. 2(b) and (d)] interacting only with the BP. Equation (1), originally developed for MOS capacitors, can also be used for MIM structures by neglecting the semiconductor capacitance (i.e., with a boundary condition $Y(0) = 0$). Fig. 4 compares the TCAD results in terms of conductance G (a), capacitance C (b) and the corresponding $\tan\delta$ (c) with those of (1), in which $\tau(x) = \tau_0 e^{2\kappa x}$, κ is modeled through the WKB approximation (see caption of Fig. 4) and τ_0 is used as the unique fitting parameter [29].

Fig. 4(a) shows that (1) accurately reproduces the conductance G of the TCAD simulation over the whole range of AC frequencies f for both capacitors. Here, we reported G/f to highlight how G increases with f [27], [29], and the G/f curves exhibit a slight decrease with f, thus indicating that G increases sublinearly with f. Also the normalized capacitance is well reproduced by (1) [Fig. 4(b)]. The relative decrease of the MOS capacitance is much larger than in the MIM. In fact, in this latter the capacitance due to traps compares to only the oxide capacitance C_{ox}, while in the former case it compares to the series of C_{ox} and the semiconductor capacitance C_S [29], hence to a smaller equivalent capacitance. This results in a wider C decay over many frequency decades for the MOS, while in the MIM, the decrease is smaller and mainly concentrated in the first f decades. Finally, Fig. 4(c) compares the simulated $\tan\delta$ and the (1) results. Note that $\tan\delta$ follows quite closely the shape of the G/f curves in (a), thus indicating that the main information on $\tan\delta$ is enclosed in the G/f curve, hence in the G increase with f. In the MOS case, $\tan\delta$ is flatter, also reflecting the more gradual C decrease over f [2].

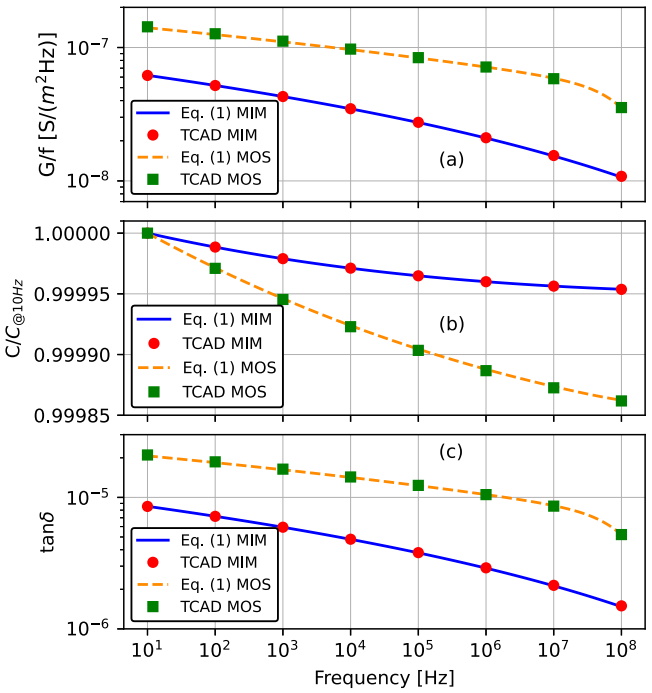

Fig. 4. (a) G/f, (b) normalized C, and (c) $\tan\delta$ calculated through TCAD (symbols) and fit with (1) (lines) for the MIM and MOS capacitors. T = 300 K and $N_{BT} = 10^{17}$ eV^{-1}cm^{-3} is uniform in energy and space. For the MOS device (green squares), Si doping is 10^{18} cm^{-3} corresponding to C_S = 18 mF/m^2 (estimated from TCAD simulation). In (1), we impose $\tau(x) = \tau_0 e^{2\kappa x}$, where $\kappa = \hbar^{-1}\sqrt{2m_t m_0(E_C - E)}$, and flat-band conditions as in [29]. Best fit of the TCAD simulation is obtained for $\tau_0 = 8\cdot10^{-10}$ s for the MOS, and $\tau_0 = 2\cdot10^{-14}$ s for the MIM.

In summary, when considering only charge exchange between traps and the BP, TCAD simulations and (1) agree well, for both MIM and MOS capacitors, in the whole explored f range, but it is worth recalling again that the model of [29] relies on the empirical parameter τ_0, assumes flat-band conditions, and it is typically used with uniform N_{BT}, confirming the need for a more general DA model. As a last remark, all the results in this section confirm that TCAD results can be considered a dependable benchmark for the DA model developed in the next section.

III. Model for Capacitance and Conductance Versus Frequency

We assume that the border traps induce small perturbations in the total capacitor admittance [36]. The equivalent circuit for traps distributed along the oxide is reported in Fig. 5(a). The oxide capacitance per unit area without traps is $C_{ox} = \varepsilon_{ox}/t_{ox}$, where t_{ox} is the oxide thickness, and it is divided into infinitesimal portions $\varepsilon_{ox}/\Delta x$ in correspondence with the trap locations. The admittances connecting the traps to both the electrodes of the capacitor are represented by ΔY_{BT} (trap to BP) and $\Delta Y_{BT}'$ (trap to TP).

When considering a single trap located at x and with an energy E, exchanging charge only with one capacitor plate (typical case for a thick oxide), the equivalent circuit is that in Fig. 5(b), where ΔY_{BT} is modeled as a series connection of a conductance ΔG_{BT} and a capacitance ΔC_{BT} [29]. Following

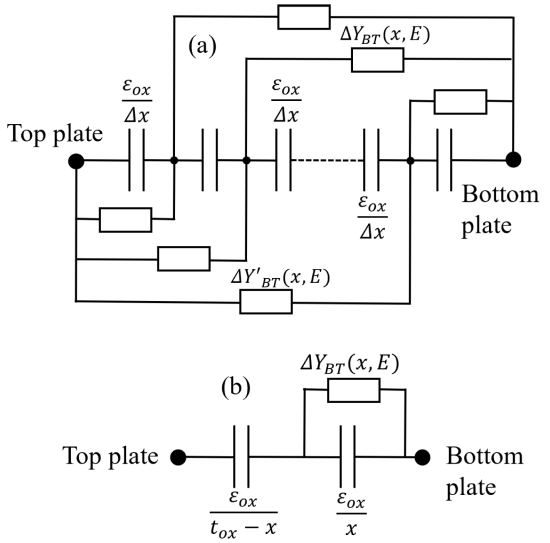

Fig. 5. (a) Equivalent circuit for traps distributed along the oxide of the capacitor. (b) Equivalent circuit used to derive the model when a trap exchanges charge with only the BP. The oxide capacitance C_{ox} is divided into ε_{ox}/x and $\varepsilon_{ox}/t_{ox} - x$ in correspondence of the trap located at x.

[32], the capacitance variation per unit volume and energy is:

$$\Delta C_{BT}(x,E) = q^2 \frac{f_0(1-f_0)}{kT} N_{BT}(x,E) \tag{7}$$

where q is the electron charge. Then, we have $\Delta G_{BT} = \Delta C_{BT}/\tau$, where $\tau(x,E)$ is again the characteristic trap time already used in (1) and (6) [29], [32]. So ΔY_{BT} can be written as

$$\Delta Y_{BT}(x,E) = \frac{\omega^2\tau\Delta C_{BT}\Delta x\Delta E}{1+(\omega\tau)^2} + j\frac{\omega\Delta C_{BT}\Delta x\Delta E}{1+(\omega\tau)^2} \tag{8}$$

where Δx and ΔE are the discretization steps in space and energy, respectively.

On the other hand, the total admittance of the circuit shown in Fig. 5(b) is given by

$$Y = \frac{j\omega\frac{\varepsilon_{ox}}{t_{ox}-x}\cdot\left(\frac{j\omega\varepsilon_{ox}}{x}+\Delta Y_{BT}\right)}{j\omega\frac{\varepsilon_{ox}}{t_{ox}-x}+\frac{j\omega\varepsilon_{ox}}{x}+\Delta Y_{BT}} \tag{9}$$

and, by separating the real and imaginary parts of (9), we get

$$Y = \frac{x^2\Delta Y_{BT}}{t_{ox}^2(1+\beta)} + j\left[\frac{\omega\varepsilon_{ox}}{t_{ox}(1+\beta)} + \frac{x^2(t_{ox}-x)\Delta Y_{BT}}{\omega\varepsilon_{ox}t_{ox}^2(1+\beta)}\right] \tag{10}$$

where

$$\beta = \left[\frac{x(t_{ox}-x)\Delta Y_{BT}}{\omega\varepsilon_{ox}t_{ox}}\right]^2. \tag{11}$$

Since the border traps are expected to represent a small perturbation with respect to the whole capacitor, we can assume $\beta \ll 1$, which leads to

$$Y = j\omega\frac{\varepsilon_{ox}}{t_{ox}} + \left(\frac{x}{t_{ox}}\right)^2\left(\frac{\omega^2\tau\Delta C_{BT}}{1+(\omega\tau)^2} + j\frac{\omega\Delta C_{BT}}{1+(\omega\tau)^2}\right)\Delta x\Delta E. \tag{12}$$

Thanks to the assumed perturbative approach, the conductance given by all the traps interacting with the BP is evaluated

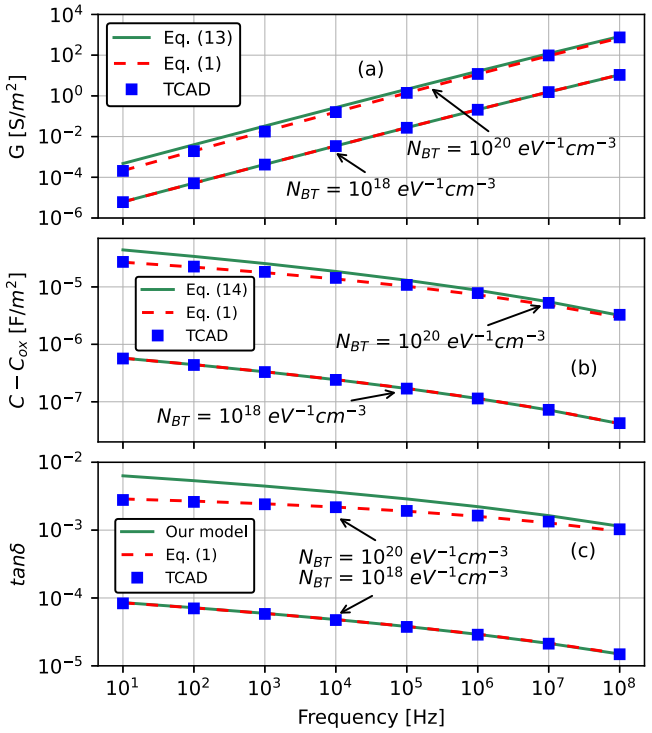

Fig. 6. Comparison of G (a), ΔC (b), and $\tan\delta$ (c) of the MIM capacitor, computed either by (13) and (14) (green solid line) or 1 [29] (red dashed line) or TCAD (symbols). Traps are uniformly distributed in energy and space and interact only with the BP.

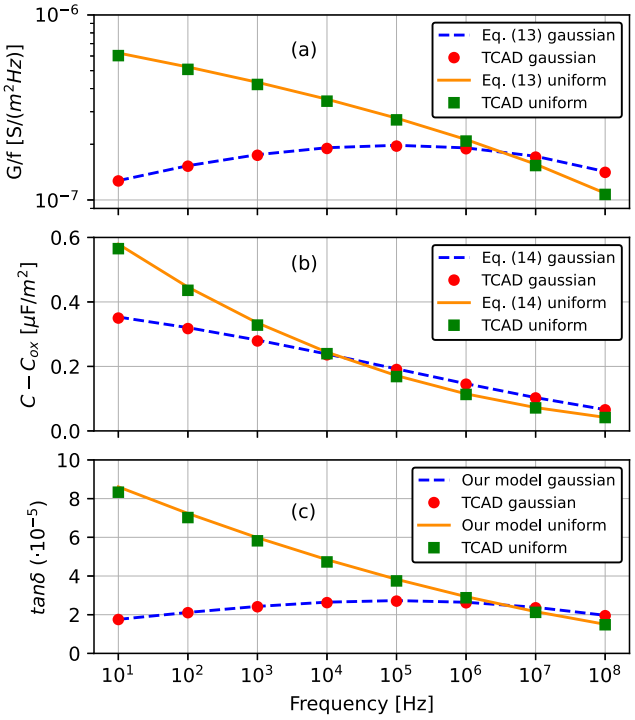

Fig. 7. TCAD simulations of the MIM capacitor and the results of (13) and (14) for uniform $N_{\rm BT}$ as in Fig. 2(b) (green squares) or with a Gaussian profile in space as in Fig. 2(c) (red circles). Trap distribution in energy is uniform for both simulations. Panel (a) shows the G/f curve, (b) capacitance increase with respect to $C_{\rm ox}$, and panel (C) the $\tan\delta$ curve.

starting from the real part of Y and integrating it over energy and space

$$G = \iint \Re\{Y\}\,dxdE = \iint \frac{x^2\omega^2\tau\Delta C_{\rm BT}}{{t_{\rm ox}}^2\left(1+\omega^2\tau^2\right)}dxdE. \quad (13)$$

Similarly, the capacitance contribution due to the traps is obtained by integrating in space and energy the imaginary part of Y as

$$\Delta C = \iint \left(\frac{\Im\{Y\}}{\omega} - C_{\rm ox}\right)dxdE = \iint \frac{x^2\Delta C_{\rm BT}}{{t_{\rm ox}}^2\left(1+\omega^2\tau^2\right)}dxdE. \quad (14)$$

Now, by combining (7), (13), and (14) calculating τ from (3) and (6), it is possible to predict the DA induced in a capacitor by a whatever trap distribution $N_{\rm BT}(x, E)$.

The equations above account for the contribution of traps interacting solely with the BP. For traps coupled with the TP, equations almost identical to (13) and (14) are obtained, in which the term $(t_{\rm ox} - x)$ replaces the term x and $\Delta C_{\rm BT}$ and τ are evaluated at the TP (i.e., the tunneling is from/to TP to/from traps and the Fermi energy to be used in (6) is the one of the TP). These additional contributions to ΔC and G are then added to (13) and (14) to obtain the total DA due to traps interacting with both the electrodes. The proposed model can also be applied to a MOS capacitor by just adding in series the semiconductor capacitance $C_{\rm S}$ to the total oxide capacitance [which includes the trap contribution described by (14)].

IV. Model Validation and Results

First, Fig. 6 compares the results from (13) and (14) with (1) and TCAD simulations for two trap densities $N_{\rm BT}$ uniformly distributed in energy and space near the BP as in Fig. 2(b) and (d). Here, for the sake of a fair comparison, $\tau(x, E)$ calculated through (3) and (6) is used in (13) and (14), but also in (1). The three approaches agree well, validating the proposed model, especially for low $N_{\rm BT}$. For high trap densities, the assumption that traps induce a small perturbation to the total admittance is not valid, leading to small differences between our model and TCAD results.

Then, Fig. 7 compares our model against TCAD simulations for different trap distributions in space: 1) uniform $N_{\rm BT} = 10^{18}$ eV^{-1}cm^{-3} (red circles) and 2) Gaussian profile with peak $2\cdot10^{18}$ eV^{-1}cm^{-3} at the BP/SiO$_2$ interface (green squares).

The $N_{\rm BT}$ values have been selected to ensure the same total number of traps in the two cases. Fig. 7, highlights how the two spatial distributions lead to a markedly different frequency dependence of the G/f curve (a) and, thus, of $\tan\delta$ (c). In particular, the Gaussian distribution results in a more constant G/f and $\tan\delta$ across the simulated frequency range, compared to the uniform $N_{\rm BT}$ case that shows a G/f and $\tan\delta$ decreasing with f. The flat G/f in Fig. 7(a) (red circles) indicates a G increasing almost linearly with f, also resulting in a quite linear decrease of C over the frequency decades [Fig. 7(b)] [2]. Fig. 7 demonstrates not only the validity of our model for various trap profiles, but also that different $N_{\rm BT}(x, E)$ produce different $\tan\delta$ trends over f.

Fig. 8 confirms that our model agrees well with the TCAD also for traps uniform in space near the BP/SiO$_2$ interface, but distributed in energy following a Gaussian profile with peak 10^{18} eV^{-1}cm^{-3}, $\sigma = 1$ eV and placed 0.5 eV below the Fermi level at the BP/SiO$_2$ interface. Note that in Fig. 8(b)

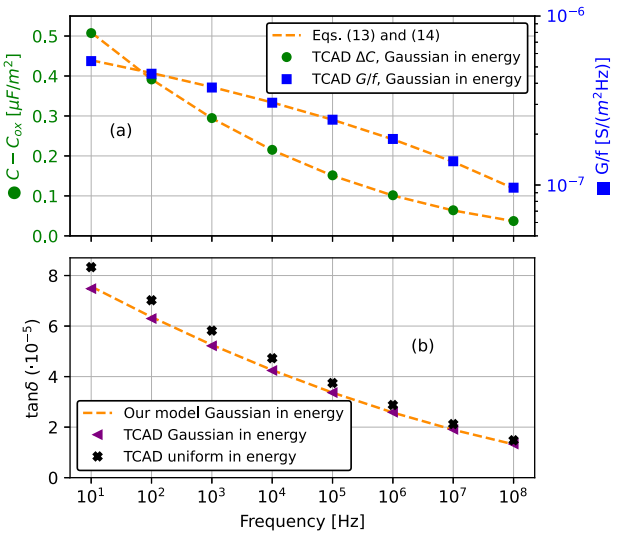

Fig. 8. (a) G/f and ΔC of the MIM stack for N_{BT} with Gaussian profile in energy and uniform in space. (b) $\tan\delta$ from the data in (a). The TCAD results for traps uniform in energy are also reported as a reference (black cross).

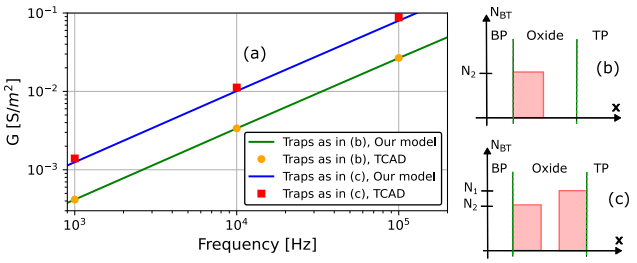

Fig. 9. (a) G from TCAD simulations is compared with our model for a MIM capacitor. Green line and yellow dots: traps only at the BP/SiO_2 interface (b) ($N_2 = 10^{18}$ eV^{-1}cm^{-3}). Blue line and red symbols: traps at both sides (c) with density $N_2 = 10^{18}$ eV^{-1}cm^{-3} at the BP/SiO_2 interface and $N_1 = 2\cdot10^{18}$ e$V^{-1}cm^{-3}$ at the TP/SiO_2 interface.

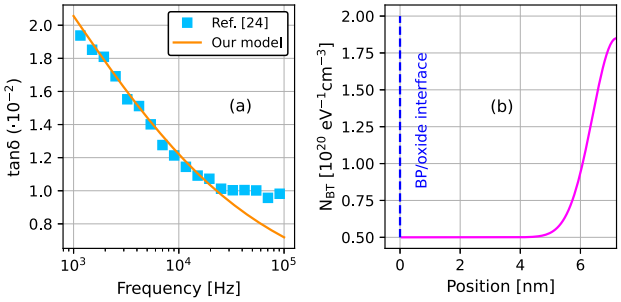

Fig. 10. (a) Experimental $\tan\delta$ of [24] and model consisting of (13) and (14) with calibrated parameters. (b) Space trap profile used to reproduce the experiments: a constant baseline of $5\cdot10^{19}$ eV^{-1}cm^{-3} is superimposed to a Gaussian tail ($1.35\cdot10^{20}$ eV^{-1}cm^{-3} peak at 7.2 nm from the $LaNiO_3/HfO_2$ interface, σ = 0.8 nm). Traps are uniform in energy between 0.5 and −1.5 eV with respect to E_F in the BP. Tunneling parameters are: S = 17, $\hbar\omega$ = 70 meV, m_t = 0.2, $V_T = 10^{-19}$ cm^3, and $LaNiO_3/HfO_2$ tunneling barrier 0.9 eV [31].

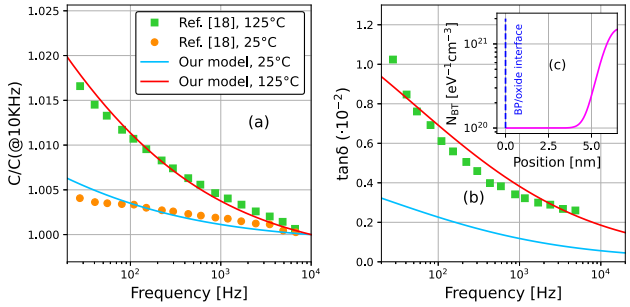

Fig. 11. (a) Normalized experimental capacitance of [18] reproduced by 14. (b) $\tan\delta$ of [18] and model consisting of (13) and (14) with calibrated parameters. (c) Extracted space trap profile: a constant baseline of 10^{20} eV^{-1}cm^{-3} is superimposed to a Gaussian tail ($1.4\cdot10^{21}$ eV^{-1}cm^{-3} peak at 6.6 nm from the TiN/Ta_2O_5 interface, σ = 0.75 nm). Traps are uniform in energy between 0.1 and 1.5 eV with respect to E_F in the BP. Tunneling parameters are: S = 12, $\hbar\omega$ = 60 meV, m_t = 0.45, $V_T = 10^{-19}$ cm^3, and 0.8 eV tunneling barrier [37], [38], [39].

the Gaussian distribution (triangles) leads to a $\tan\delta$ trend very similar to that due to a uniform trap distribution in energy (black crosses, reported as a reference). This suggests that the $\tan\delta$ versus f behavior is primarily governed by the trap's spatial distribution. This is because the dominant DA contribution comes from traps located at the BP Fermi level [29] and, in the two distributions, $N_{BT}(x, E_F)$ is very similar, thus leading to comparable $\tan\delta$ values for both simulations.

Fig. 9(a) compares G calculated through our model and the TCAD, considering two scenarios: traps exchanging charge only with the BP (green line and yellow dots), and traps interacting with both electrodes (blue line and red symbols). Traps are uniformly distributed in energy and space near each interface [Fig. 9(b) and (c)]. The good agreement demonstrates how the proposed model correctly handles also the more general case in which traps interact with both capacitor plates.

To prove the capability of our model to reproduce experiments, allowing the extraction of the trap spatial distribution from DA experiments, in Fig. 10(a), we adjusted the trap parameters to match the measured $\tan\delta$ on the HfO_2-based MIM of [24]. Our model reproduces well the data by using the spatial trap distribution in Fig. 10(b). Fig. 11 shows that (14) can accurately reproduce also measurements for MIM capacitors (Ta_2O_5 dielectric) at different temperatures [18] by a proper tuning of the spatial and energy distribution of traps [Fig. 11(c)]. Indeed, by using the same trap profile, the model reproduces the C (Fig. 11(a), two temperatures) and $\tan\delta$ values (b). Experimental $\tan\delta$ is available only for T = 125 °C [18], but for completeness, the simulated $\tan\delta$ at T = 25 °C is shown too. The trap profile in Fig. 11(c) is qualitatively similar to that reported in [40] for the same device. Note that, in the explored f range, the portion of the trap distribution contributing to the DA is shown in Figs. 10(b) and 11(c). A finer tuning of the parameters to improve the matching in Figs. 10 and 11 is beyond the scope of this work. It is also worth noticing that reproducing data at different T with the model of [29] would require adjusting empirically τ with T and probably defining an effective N_{BT} changing with T.

V. Conclusion

A model describing the DA effects on MIM/MOS capacitors due to border traps with arbitrary distribution in energy and space and interacting with both capacitor plates has been developed and extensively validated through TCAD simulations. The model has also been used to interpret experimental results, extracting the trap profiles. The proposed formulation effectively extends the capability of available DA models.

Concerning the simulation results, the increase of G in frequency mainly determines the $\tan\delta$ versus f trend, also suggesting that the capacitance value plays a marginal role in the $\tan\delta$ behavior. Furthermore, the spatial trap distribution largely impacts the $\tan\delta$ versus f trend, showing a decreasing $\tan\delta$ for traps uniformly distributed, whereas a trap density lowering toward the oxide depth results in a flatter $\tan\delta$.

REFERENCES

[1] M. Kropfitsch, P. Riess, G. Knoblinger, and D. Draxelmayr, "Dielectric absorption of low-k materials: Extraction, modelling and influence on SAR ADCs," in *Proc. IEEE Int. Symp. Circuits Syst.*, Jun. 2006, pp. 1–4, doi: 10.1109/ISCAS.2006.1692643.

[2] S. Saro et al., "Compact expression to model the effects of dielectric absorption on analog-to-digital converters," in *Proc. IEEE 36th Int. Conf. Microelectronic Test Struct. (ICMTS)*, Apr. 2024, pp. 1–5, doi: 10.1109/ICMTS59902.2024.10520681.

[3] L. Michaeli, J. Šaliga, P. Dolinský, and I. Andráš, "Compensation of dual slope ADC error caused by dielectric absorption," in *Proc. 11th Int. Conf. Meas.*, 2017, pp. 63–66, doi: 10.23919/measurement.2017.7983536.

[4] J. C. Kuenen and G. C. M. Meijer, "Measurement of dielectric absorption of capacitors and analysis of its effects on VCOs," *IEEE Trans. Instrum. Meas.*, vol. 45, no. 1, pp. 89–97, Jan. 1996, doi: 10.1109/19.481317.

[5] R. Karthik and A. Akshaykranth, "Fabrication and modeling of multi-layer metal–insulator-metal capacitors," *J. Semicond.*, vol. 38, no. 12, Nov. 2017, Art. no. 123002, doi: 10.1088/1674-4926/38/12/123002.

[6] R. W. Sillars, "The properties of a dielectric containing semiconducting particles of various shapes," *J. Inst. Electr. Eng.*, vol. 80, no. 484, pp. 378–394, Apr. 1937, doi: 10.1049/jiee-1.1937.0058.

[7] K. Kundert, "Modeling dielectric absorption in capacitors," Tech. Rep., Jan. 2004. [Online]. Available: https://designers-guide.org/modeling/da.pdf

[8] Z. Xu et al., "A study of relaxation current in high-κ dielectric stacks," *IEEE Trans. Electron Devices*, vol. 51, no. 3, pp. 402–408, Mar. 2004, doi: 10.1109/TED.2003.822343.

[9] H. Muminovic, P. Riess, P. Baumgartner, and P. Klein, "Temperature dependent dielectric absorption characterization and modeling for SiN, Al_2O_3 and Ta_2O_5," in *Proc. Eur. Solid State Device Res. Conf.*, Sep. 2010, pp. 293–296, doi: 10.1109/essderc.2010.5618355.

[10] K. E. K. Holden et al., "Dielectric relaxation, aging and recovery in high-K MIM capacitors," in *Proc. IEEE Int. Rel. Phys. Symp. (IRPS)*, Mar. 2021, pp. 1–10, doi: 10.1109/IRPS46558.2021.9405212.

[11] D. M. Fleetwood, "'Border traps' in MOS devices," *IEEE Trans. Nucl. Sci.*, vol. 39, no. 2, pp. 269–271, Apr. 1992, doi: 10.1109/23.277495.

[12] Z. Ning et al., "Dielectric relaxation of MIM capacitor and its effect on sigma-delta A/D converters," *IEEE Trans. Semicond. Manuf.*, vol. 21, no. 4, pp. 549–564, Nov. 2008, doi: 10.1109/TSM.2008.2004339.

[13] P. Zhao et al., "Evaluation of border traps and interface traps in HfO_2/MoS_2 gate stacks by capacitance–voltage analysis," *2D Mater.*, vol. 5, no. 3, Apr. 2018, Art. no. 031002, doi: 10.1088/2053-1583/aab728.

[14] O. Khaldi, F. Jomni, P. Gonon, C. Mannequin, and B. Yangui, "Investigation of electrical properties of HfO_2 metal–insulator–metal (MIM) devices," *Appl. Phys. A, Solids Surf.*, vol. 116, no. 4, pp. 1647–1653, Sep. 2014, doi: 10.1007/s00339-014-8292-8.

[15] H. Hu, C. Zhu, Y. F. Lu, M. F. Li, B. Jin Cho, and W. K. Choi, "A high performance MIM capacitor using HfO_2 dielectrics," *IEEE Electron Device Lett.*, vol. 23, no. 9, pp. 514–516, Sep. 2002, doi: 10.1109/LED.2002.802602.

[16] R. Thomas, D. C. Dube, M. N. Kamalasanan, S. Chandra, and A. S. Bhalla, "Structural, electrical, and low-temperature dielectric properties of sol–gel derived $SrTiO_3$ thin films," *J. Appl. Phys.*, vol. 82, no. 9, pp. 4484–4488, Nov. 1997, doi: 10.1063/1.366181.

[17] C. Ng, K. Chew, J. Li, T. Tjoa, L. Goh, and S. Chu, "Characterization and comparison of two metal-insulator-metal capacitor schemes in 0.13 μm copper dual Damascene metallization process for mixed-mode and RF applications," in *IEDM Tech. Dig.*, Jul. 2002, pp. 241–244, doi: 10.1109/IEDM.2002.1175822.

[18] J.-P. Manceau et al., "Dielectric relaxation characterization and modeling in large frequency and temperature domain: Application to fF/μm^2 Ta_2O_5 MIM capacitor," in *Proc. IEEE Int. Conf. Microelectronic Test Struct.*, Jun. 2006, pp. 199–204, doi: 10.1109/ICMTS.2006.1614303.

[19] J.-P. Manceau, S. Bruyere, S. Jeannot, A. Sylvestre, and P. Gonon, "Leakage current variation with time in Ta_2O_5 MIM and MIS capacitors," in *Proc. IEEE Int. Integr. Rel. Workshop Final Rep.*, Oct. 2006, pp. 129–133, doi: 10.1109/IRWS.2006.305226.

[20] X. Yu et al., "A high-density MIM capacitor (13 fF/μm^2) using ALD HfO_2 dielectrics," *IEEE Electron Device Lett.*, vol. 24, no. 2, pp. 63–65, Feb. 2003, doi: 10.1109/LED.2002.808159.

[21] J. Mu, X. Chou, Z. Ma, J. He, and J. Xiong, "High-performance MIM capacitors for a secondary power supply application," *Micromachines*, vol. 9, no. 2, p. 69, Feb. 2018, doi: 10.3390/mi9020069.

[22] A. Raja, R. Laibowitz, E. G. Liniger, T. M. Shaw, and T. F. Heinz, "Impedance spectroscopy studies of moisture uptake in low-k dielectrics and its relation to reliability," *Microelectronic Eng.*, vol. 147, pp. 100–103, Nov. 2015, doi: 10.1016/j.mee.2015.04.020.

[23] A. Goswami and A. P. Goswami, "Dielectric and optical properties of ZnS films," *Thin Solid Films*, vol. 16, no. 2, pp. 175–185, May 1973, doi: 10.1016/0040-6090(73)90166-1.

[24] L. Zhang et al., "ALD preparation of high-k HfO_2 thin films with enhanced energy density and efficient electrostatic energy storage," *RSC Adv.*, vol. 7, no. 14, pp. 8388–8393, 2017, doi: 10.1039/c6ra27847g.

[25] M. K. Hota, C. K. Sarkar, and C. K. Maiti, "Frequency-dependent dielectric response of $HfTaO_x$-based metal–insulator–metal capacitors," *Semicond. Sci. Technol.*, vol. 27, no. 8, Jun. 2012, Art. no. 085002, doi: 10.1088/0268-1242/27/8/085002.

[26] D. E. Yıldız, M. Yıldırım, and M. Gökçen, "Investigation on dielectric properties of atomic layer deposited Al_2O_3 dielectric films," *J. Vac. Sci. Technol. A, Vac., Surf., Films*, vol. 32, no. 3, May 2014, Art. no. 031509, doi: 10.1116/1.4870593.

[27] H. Preier, "Contributions of surface states to MOS impedance," *Appl. Phys. Lett.*, vol. 10, no. 12, pp. 361–363, Jun. 1967, doi: 10.1063/1.1728213.

[28] P. C. Dow, "An analysis of certain errors in electronic differential analyzers II-capacitor dielectric absorption," *IRE Trans. Electron. Comput.*, vol. EC-7, no. 1, pp. 17–22, Mar. 1958, doi: 10.1109/TEC.1958.5222090.

[29] Y. Yuan et al., "A distributed model for border traps in *Al_{2} O_{3}-InGaAs* MOS devices," *IEEE Electron Device Lett.*, vol. 32, no. 4, pp. 485–487, Apr. 2011, doi: 10.1109/LED.2011.2105241.

[30] *SentaurusT Device User Guide*, Synop., Sunnyvale, CA, USA, Sep. 2024.

[31] L. Vandelli, A. Padovani, L. Larcher, R. G. Southwick, W. B. Knowlton, and G. Bersuker, "A physical model of the temperature dependence of the current through SiO_2/HfO_2 stacks," *IEEE Trans. Electron Devices*, vol. 58, no. 9, pp. 2878–2887, Sep. 2011, doi: 10.1109/TED.2011.2158825.

[32] E. H. Nicollian and J. R. Brews, *MOS (Metal Oxide Semiconductor) Physics and Technology*. New York, NY, USA: Wiley, 1982.

[33] M. I. Vexler, S. E. Tyaginov, and A. F. Shulekin, "Determination of the hole effective mass in thin silicon dioxide film by means of an analysis of characteristics of a MOS tunnel emitter transistor," *J. Phys., Condens. Matter*, vol. 17, no. 50, pp. 8057–8068, Dec. 2005, doi: 10.1088/0953-8984/17/50/023.

[34] I. T. Godmanis, A. N. Trukhin, and K. Hübner, "Exciton–phonon interaction in crystalline and vitreous SiO_2," *Phys. Status Solidi (B)*, vol. 116, no. 1, pp. 279–287, Mar. 1983, doi: 10.1002/pssb.2221160133.

[35] A. Palma, J. A. López-Villanueva, and J. E. Carceller, "Electric field dependence of the electron capture cross section of neutral traps in SiO_2," *J. Electrochemical Soc.*, vol. 143, no. 8, pp. 2687–2690, Aug. 1996, doi: 10.1149/1.1837072.

[36] F. P. Heiman and G. Warfield, "The effects of oxide traps on the MOS capacitance," *IEEE Trans. Electron Devices*, vol. ED-12, no. 4, pp. 167–178, Apr. 1965, doi: 10.1109/T-ED.1965.15475.

[37] S. Yildirim, K. Ulutas, D. Deger, E. O. Zayim, and I. Turhan, "Dielectric properties of sol–gel derived Ta_2O_5 thin films," *Vacuum*, vol. 77, no. 3, pp. 329–335, Feb. 2005, doi: 10.1016/j.vacuum.2004.12.002.

[38] R. Brazis, P. Pipinys, A. Rimeika, and V. Lapeika, "Electron transport in Ta_2O_5 films," *J. Mater. Sci. Lett.*, vol. 9, no. 3, pp. 266–267, Mar. 1990, doi: 10.1007/bf00725819.

[39] S. Venica, F. Driussi, P. Palestri, and L. Selmi, "Graphene base transistors with optimized emitter and dielectrics," in *Proc. 37th Int. Conv. Inf. Commun. Technol., Electron. Microelectron. (MIPRO)*, May 2014, pp. 33–38, doi: 10.1109/MIPRO.2014.6859528.

[40] E. Deloffre, C. Wyon, and M. Gros-Jean, "Investigation and characterization of mim structures based on mocvd and pealed Ta_2O_5 films," in *Proc. ECS Meeting Abstr.*, Feb. 2006, no. 9, p. 434, doi: 10.1149/MA2005-01/9/434.